Peer-reviewed version available at Entropy 2018, 20, 705; doi:10.3390/e20090705

Spatial Organization of Five-Fold Morphology as a Source of Geometrical Constraint in Biology

Juan López-Sauceda [1,2,*], Jorge López-Ortega [2], Gerardo Abel Laguna Sánchez [2], Jacobo Sandoval Gutiérrez [2], Ana Paola Rojas Meza [2] and José Luis Aragón-Vera [3]

[1] Mexican National Council for Science and Technology (CONACYT, Mexico). Full postal address; Av. Insurgentes Sur 1582, Col. Crédito Constructor, Zip code 03940, Mexico City, Mexico
[2] Department of Information Systems and Computational Sciences, Universidad Autónoma Metropolitana, Unidad Lerma. Full postal address; Av. Hidalgo Pte. 46, Col. La Estación, Zip code 52006, Lerma de Villada, Estado de Mexico, Mexico
[3] Department of nanotechnology. Universidad Nacional Autónoma de México. Campus Juriquilla. Full postal address; Av. Blvd. Juriquilla 3001, Col. Juriquilla la Mesa, Zip code 76230, Juriquilla, Queretaro, Mexico
* Correspondence: j.lopez@correo.ler.uam.mx; Tel.: +52-5553760012

Abstract: A basic pattern in the body plan architecture of many animals, plants and some molecular and cellular systems is five-part units. This pattern has been understood as a result of genetic blueprints in development and as a widely conserved evolutionary character. Despite some efforts, a definitive explanation of the abundance of pentagonal symmetry at so many levels of complexity is still missing. Based on both, a computational platform and a statistical spatial organization argument, we show that five-fold morphology is substantially different from other abundant symmetries like three-fold, four-fold and six-fold symmetries in terms of spatial interacting elements. We develop a measuring system to determine levels of spatial organization in 2D polygons (homogeneous or heterogeneous partition of defined areas) based in principles of regularity in a morphospace. We found that spatial organization of five-fold symmetry is statistically higher than all other symmetries studied here (three to ten-fold symmetries) in terms of spatial homogeneity. The significance of our findings is based on the statistical constancy of geometrical constraints derived from spatial organization of shapes, beyond the material or complexity level of the many different systems where pentagonal symmetry occurs.

Keywords: Pentagon; fivefold morphology; body plan; spatial organization; morphospace.

1. Introduction

One of the most conspicuous properties in many biological systems is the pentagonal symmetry **[1]**. There are many notable examples of pentagonal symmetry in the members of some biological groups like Echinodermata, radiolarians, flowering plants and some fruits. In many cases, the five-fold symmetry is clearly displayed but in some others the radial symmetry is lost and it only remains a bilateral symmetry. In this last case, however the body is still divided into five parts. For this reason, we relax the restriction of symmetry and in both cases we will say that the structure displays five-fold organization (FO) which in terms of phenotype is uncovered as fivefold symmetry. These five-part units are very common in both animal and plant design and, traditionally, in biology this design symmetry and their emergence have been approached by developmental genetics, evolutionary biology and ecology [2, 3, 4, 5, 6, 7, 8, 9 and 10]. In spite of its abundance in nature, there are few general comments on the extended frequency of FO as a shape, with some important exceptions [10 and 11]. In a pioneering work, Breder [11] shows that FO is the basic pattern of many flowers, dicotyledons, echinoderms, the vertebrate body section, the distal ends of tetrapod limbs, and of the oral armature of priapulids. Breder concludes "Five-partness, where it appears, is held to with great rigidity, even when extensive evolutionary change has taken place. This does not seem to be the case to such a marked extent where other symmetries are concerned, as the coelenterates witness". The reasons for the success of FO, where it appears, are not

yet understood. In a biological context, some hypotheses have been formulated in sea urchins and flowers, either based on their functional, ecological role, developmental constraints [7, 8,9, 13, 14 and 15] or its robustness and formation derived from mechanical [16] or mathematical models [17]. However, if these hypotheses are true they do not explain the occurrence and robustness of FO in all other organisms and in the remaining non-organismic entities such as molecules, cellular and inorganic organizations. Breder [11] suggested that the origin of the stability of the FO lies in the geometrical properties of the pentagon.

Convex polygons are plane entities and their geometry restricts the way inner regions (considered as sub-entities) are partitioned. These surface regions distribute areas inside polygons and, with a proper measure of spatial organization in 2D shapes, a measure of that distribution can be determined. In fact, an important constraint in any spatial region may be the spatial homogeneity or regularity. In general, the absence of spatial disparity among areas inside a region (a bounded polygon) is considered synonymous of regularity and the presence of disparity is considered spatial heterogeneity. Therefore, our definition of spatial heterogeneity is based on the unequal distribution of areas inside polygons. We propose a parameter to define quantitatively the spatial organization of polygonal constituent elements according to this couple of concepts. It has been shown in a previous work [18] that eutacticity is a parameter closely linked with regularity and it is a suitable measurement of spatial homogeneity and heterogeneity. That regularity is derived from measures of variation of partitioning areas. The spontaneous organization of individual blocks into ordered structures is ubiquitous in nature and found at all length scales, thus the shape of the building blocks becomes increasingly important [19 and 20]. The analysis of abstract entities, such as the geometry of these building blocks, into constituent elements and their degrees of interaction among internal parts represents a source of important information in terms of constrictions and evolvability [21]. This approach is called modularity. It is assumed that systems are composed by individual elements or *modules* and knowledge of modules and their integration is important to understand some properties of these particular systems. This concept can be a useful tool to infer features on the way organisms or generic systems are build, for instance due to organizational principles of self-maintaining systems [22], or it may be an "evolved property" [21]. In this work, we study the problem of the high frequency of FO in nature by using the concept of module in simple polygonal organizations. Intuitively, here, a module is a summation of particular elements from many polygons and it will depict non trivial differences between shapes, in terms of spatial organization, inside a universe of shapes or star morphospace. Thus, our main aim is the analysis of FO partitioning in order to understand not just the description of modules in a generic morphospace of stars, but the proposal of a plausible hypothesis regarding the high occurrence of FO in terms of spatial efficiency.

A theoretical morphospace has been used in an evolutionary context as a geometric space of both existent and non-existent biological forms [23]. An important step towards the proof that spatial efficiency is related with the high occurrence of FO, is the developing of a morphospace of stars with different symmetries. The goal in this case will be to show that FO is restricted to a particular zone of spatial homogeneity inside the morphospace. Therefore, we claim that spatial organization should be considered an important way to find how existent shapes appears in the morphological context of phenotypes or generic spatial organizations in nature.

The rest of the paper is distributed as follows: Section 3.1 of Methods shows the statistical basis of spatial homogeneity and heterogeneity for our work: We introduce two statistical parameters defining the variability of areas inside polygons, which, in turn, will define particular spatial configurations. Section 3.2 is about the mathematical basis of eutacticity, based on previous references [24 and 25]. Our numerical proof in Section 3.3 and 3.4 will define the amplitude of spatial variability of sub-elements in polygons derived from stars, called modules, showing the association between eutacticity and our statistical argument. In Section 4.1 of results, a universe of shapes Γ or star morphospace is shown and its statistical categorization is given.

Preprints (www.preprints.org) | NOT PEER-REVIEWED | Posted: 2 August 2018 doi:10.20944/preprints201808.0042.v1

Peer-reviewed version available at Entropy 2018, 20, 705; doi:10.3390/e20090705

2. Methods

Section 2.1 Statistics of spatial organization for shapes Γ.

To establish a proper measure of spatial organization we start by defining a shape Γ. A shape Γ is a set of spatial planar confined regions called sub-localities inside a locality L_i. Hence, a shape might be a regular or irregular polygon. In addition, we will see that each shape Γ can be associated to a star which, eventually, will be turned into a number (a set of area) that can be subject to be statistically analyzed. Our statistical analysis will be derived from localities and their sub-localities coming from constructions of shapes Γ. The main idea to establish the generic name of shapes Γ is because it useful to define either shapes or numbers associated with shapes.

Each locality L_i is constituted by a subset of a given number N_i of sub-localities, $S_{i1}, S_{i2}, \dots, S_{i_{Ni}}$ such that $L_i = \cup_{j=1}^{N_i} S_{ij}$, where L_i is a convex regular or irregular polygon in $\mathbb{R}^2$. Let A_{ij} be the area of each sub-locality. If $A_{ij} = A_{ik} \forall\, k, j$, then we said that L_i is regular (Figure 1). In contrast, if there exists some $j \neq k$ such that $A_{ij} \neq A_{ik}$ then we say that L_i is not regular. Therefore, let $A_i = \sum_{j=1}^{N_i} A_{ij}$ be the sum of all the associated areas of every locality; this set determines $\Gamma = \{A_i\}$. Therefore, Γ is a generalization of locality or any set of sub-localities which will be understood as a number in statistical terms. Therefore, the area average of a locality L_i is:

$$\bar{A}_i = \frac{1}{N_i} \sum_{j=1}^{N_i} A_{ij} \qquad (1)$$

and

$$\sigma_i = \sqrt{\frac{1}{N_i - 1} \sum_{j=1}^{N_i} (A_{ij} - \bar{A}_i)^2} \qquad (2)$$

is the standard deviation of each locality. Notice that if $\sigma_i = 0 \Rightarrow A_{ij} = A_{ik}\ \forall\, j, k$.

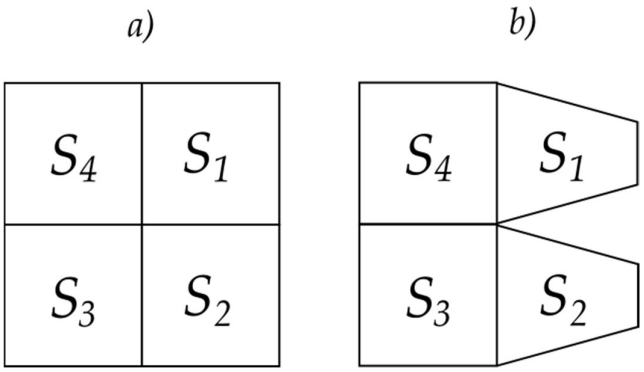

Figure 1. Schematic properties of two different shapes Γ. a) A square is a locality associated to four subareas from four sub-localities $S_1, S_2, \dots, S_4$ which are all equal. b) A shape Γ with a four-fold partition such that any of their sub-localities have unequal subareas is not regular; the set of areas defined by sub-localities S_1 and S_2 are smaller than those of S_3 and S_4.

Section 2.2 Mathematical basis of eutacticity.

A star ψ is a set of n vectors $\{u_1, u_2, \dots, u_n\}$ with a common origin in an N-dimensional space ($\mathbb{R}^N$). The star is eutactic if it can be obtained by projecting an orthogonal set. Eutacticity is sharply linked with regularity by considering that a given polygon, polyhedron and, in general, polytope can be associated with a star of vectors (pointing from the center to the vertices) and it has been

Peer-reviewed version available at Entropy 2018, 20, 705; doi:10.3390/e20090705

demonstrated that stars associated with regular polytopes are eutactic [26]. A good numerical criterion for obtaining the eutacticity of a star, suitable for dealing with experimental measurements, was proposed in Ref. [27] and is as follows. Let B be the matrix whose N columns are the coordinates of the vectors forming a star ψ, with respect to a given fixed orthonormal basis of $\mathbb{R}^2$. The star is eutactic if and only if:

$$\varepsilon = \frac{Tr(S)}{\sqrt{Tr(SS)}\sqrt{2}} = 1 \quad (3)$$

Where $S = BB^T$; Tr denotes the trace and the superindex T denotes the transpose. Notice that the parameter ε can indicate the degree of eutacticity of the star represented by B: if it is not strictly 1, which is the highest value of eutacticity, then the closer to 1 the more eutactic the star is. In case of planar stars, it can be proved that:

$$\frac{1}{\sqrt{2}} \leq \varepsilon \leq 1 \quad (4)$$

The strategy is the to associate a given polygon or locality L_i, with a star ψ, and to use Eq. 3 to measure its value of eutacticity. Next, a measure of spatial organization can be proposed and used to measure the regularity of a form Γ, using sub-locality areas. For this goal, we should prove that the closer ε is to 1, the more regular (the feature of spatial homogeneity) the star is (section 2.3). Our hypothesis is that the higher the eutacticity, the more homogeneous (*i. e.*, the area variability of the sub-locality decreases) the partition of the space is. Lower values of eutacticity imply unequal partition of the space, or more area variability or spatial heterogeneity. According to equations (1) and (2), the variability defining regularity must occur inside localities. In order to support statistical variation between highly regular stars or highly eutactic stars, in contrast with non regular stars, we need to define spatial variability between two experimental groups, highly eutactic and less eutactic stars and polygons associated with them.

Section 2.3 The eutacticity and the standard deviation of dispersion mean of a module.

The algorithms used in this section are found at reference [24]. In this section, we will show that eutacticity is an important parameter measuring spatial organization. Here, we introduce the concept of module to support the statistical framework of Section 2.1, linking this with vector stars ψ described in Section 2.2. Spatial organization is the fundamental property to quantify regularity using polygons. A partition of the localities L_i into sub-localities $S_{i1}, S_{i2}, \dots, S_{i_{Ni}}$ is proposed using Voronoi tessellations as proposed in Ref. [24]. The goal in Ref. [24] was to verify the spatial distribution of areas inside localities by comparing stars with high and low values of eutacticity. In this way, two experimental groups can be distinguished; ψ_a representing eutactic stars $(\varepsilon = 1)$ and ψ_b representing stars with a lower value of eutacticity $(\varepsilon = 0.8)$. With these two groups, we proceed as follows. There will be $\psi_1, \psi_2, \dots, \psi_k$ stars such that 1) All of them have the same value of ε; 2) Any of them has the same number of vectors ν; 3) They are geometrical random stars, even though any of them has the same eutacticity value (point 1). Finally, 4) Stars $\psi_1, \psi_2, \dots, \psi_k$ are the building blocks to construct localities $L_1, L_2, \dots, L_k$ with the number N_i of sub-localities $S_{i1}, S_{i2}, \dots, S_{i_{Ni}}$associated with the same number of vectors ν. In fact, according to the property 2, we have $N_i = N_j = \nu, \forall\, i, j$, which is an important condition to with a formal definition of module. Intuitively, a module is a summation of particular sub-localities from many localities and it will be used to contrast two arbitrary values of ε numerically (Figure 2).

Preprints (www.preprints.org) | NOT PEER-REVIEWED | Posted: 2 August 2018 doi:10.20944/preprints201808.0042.v1

Peer-reviewed version available at Entropy 2018, 20, 705; doi:10.3390/e20090705

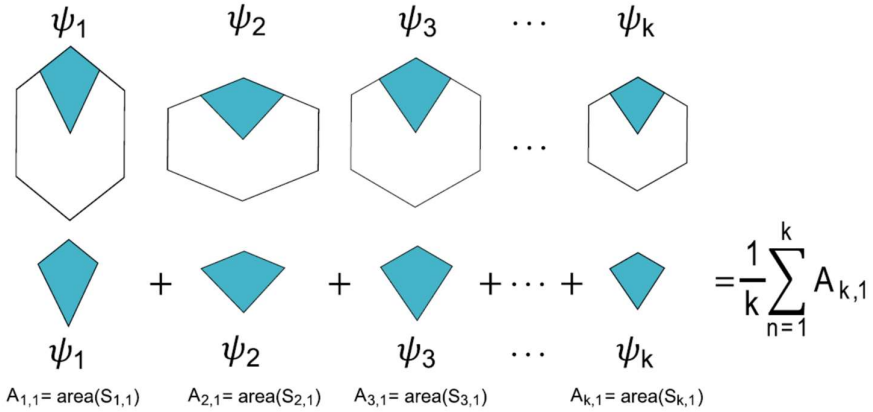

Figure 2. Construction of a module from k stars. A module is an average derived from an area summation of a particular sub-locality (e.g., sub-locality 1) from k stars ψ with a constant value ε. In this figure the second sub index of A is referring to sub-locality 1. Stars $\psi_1, \psi_2, \ldots, \psi_k$ are the building blocks to construct localities $L_1, L_2, \ldots, L_k$. This process is applied to build modules of the two experimental groups of stars, ψ_a and ψ_b. Figure modified from reference 24.

According to Ref. [24], let us assume that the areas $A_{i,j}$ associated to sub-localities of the two groups of stars (ψ_a, ψ_b) have two crucial components: a) The eutacticity ε of the star ψ and b) a set of random points $\omega_{m,n}$ defining the associated areas $A_{i,j}$. It is important to highlight that $L_1, L_2, \ldots, L_k$ depend on $\psi_1, \psi_2, \ldots, \psi_k$ (property 4 of stars ψ). According to this, $\psi_1, \psi_2, \ldots, \psi_k$ are associated with $\omega_{m,n}$ which will define regions to establish sub-localities $S_{i1}, S_{i2}, \ldots, S_{i_{Ni}}$. In that sense, let us call $\psi_{1,j}^{\omega_{1,n}}, \psi_{2,j}^{\omega_{2,n}}, \ldots, \psi_{k,j}^{\omega_{k,n}}$ to the stars, where j represents the particular sub-locality and n is the set of random points $n = 1, \ldots, \alpha$. So $\omega_{m,i} \neq \omega_{m,j}$ for every $i \neq j$. In this case, $m = 1, \ldots, k$ is a simple tag to associate star k with ω_k and subsequently with a set α of random points, and the associated areas are $A_{1,j}^{\omega_{1,n}}, A_{2,j}^{\omega_{2,n}}, \ldots, A_{k,j}^{\omega_{k,n}}$. Therefore, the module for a particular sub-locality is defined using the average of its areas. Modules for particular sub-localities of two experimental groups of stars (ψ_a, ψ_b) are built in order to contrast its sub-locality area variations.

In Table 1, an example of the analysis of module 1, which is exclusive for sub-locality 1 in a locality of j sub-localities, is shown:

Table 1: Calculation of a module for sub-locality 1.

	Set of random points $\omega_{m,n}$ defining the associated areas $A_{i,j}$ for sub-locality 1 [algorithm defined in Ref. 24].					Summation of areas for star ψ_k
Stars	$\omega_{1,1}$	$\omega_{1,2}$	…	$\omega_{1,\alpha}$		
ψ_1	$A_{1,1}^{\omega_{1,1}}$	$A_{1,1}^{\omega_{1,2}}$	…	$A_{1,1}^{\omega_{1,\alpha}}$	⇒	$\frac{1}{\alpha}\sum_{n=1}^{\alpha} A_{1,1}^{\omega_{1,n}}$
ψ_2	$A_{2,1}^{\omega_{2,1}}$	$A_{2,1}^{\omega_{2,2}}$	…	$A_{2,1}^{\omega_{2,\alpha}}$	⇒	$\frac{1}{\alpha}\sum_{n=1}^{\alpha} A_{2,1}^{\omega_{2,n}}$
.	.	.	.	.	.	.
.	.	.	.	.	.	.
.	.	.	.	.	.	.

Preprints (www.preprints.org) | NOT PEER-REVIEWED | Posted: 2 August 2018 doi:10.20944/preprints201808.0042.v1

Peer-reviewed version available at Entropy 2018, 20, 705; doi:10.3390/e20090705

ψ_k	$A_{k,1}^{\omega_{k,1}}$	$A_{k,1}^{\omega_{k,2}}$	…	$A_{k,1}^{\omega_{k,\alpha}}$	⇒	$\frac{1}{\alpha}\sum_{n=1}^{\alpha} A_{k,1}^{\omega_{k,n}}$

The summation Σ of module 1 derived from sub-locality 1 in a locality with j sub-localities, k stars and a set α of randomly generated points will be defined by:

$$\frac{1}{\alpha}\left(\sum_{n=1}^{\alpha} A_{11}^{\omega_{1n}} + \sum_{n=1}^{\alpha} A_{21}^{\omega_{2n}} + \cdots + \sum_{n=1}^{\alpha} A_{k1}^{\omega_{kn}}\right) \quad (5)$$

Therefore, the average for module 1 is:

$$\bar{A}_{\mu_1} = \frac{1}{\alpha k}\sum_{i=1}^{k}\sum_{n=1}^{\alpha} A_{i,1}^{\omega_{i,n}}$$

and the standard deviation:

$$\sigma_{\mu_1} = \sqrt{\frac{1}{(\alpha-1)(k-1)}\sum_{n=1}^{\alpha}\sum_{i=1}^{k}(A_{i1}^{\omega_{in}} - \bar{A}_{\mu})^2} \quad (6)$$

In general, for any sub-locality $A_{i,j}^{\omega_{i,n}}$ associated with the star S_i, we can obtain the average of each star and the average of each set of random points of the module A_{μ_j}. This average is:

$$\bar{A}_{\mu_j} = \frac{1}{\alpha k}\sum_{i=1}^{k}\sum_{n=1}^{\alpha} A_{i,j}^{\omega_{i,n}}$$

and the standard deviation:

$$\sigma_{\mu_j} = \sqrt{\frac{1}{(\alpha-1)(k-1)}\sum_{i=1}^{\alpha}\sum_{n=1}^{k}(A_{i,j}^{\omega_{i,n}} - \bar{A}_{\mu_j})^2} \quad (7)$$

If now we fix a star, the average of areas and standard deviation of this locality by summation over α random set of points is

$$\bar{A}_{\mu_j}(S_i) = \frac{1}{\alpha}\sum_{n=1}^{\alpha} A_{i,j}^{\omega_{i,n}}$$

And

$$\sigma_{\mu_j}(S_i) = \sqrt{\frac{1}{\alpha-1}\sum_{n=1}^{\alpha}(A_{i,j}^{\omega_{i,n}} - \bar{A}_{\mu_j}(S_i))^2} \quad (8)$$

The average of these standard deviations is calculated by performing summation over the k stars:

$$\bar{\sigma}_{\mu_j} = \frac{1}{k}\sum_{i=1}^{k}\sigma_{\mu_j}(S_i) \quad \text{(Dispersion mean of module } j\text{; 9)}$$

which will have the final standard deviation:

$$\sigma_{S\mu} = \sqrt{\frac{1}{(k-1)}\sum_{i=1}^{k}(\sigma_{\mu_j}(S_i) - \bar{\sigma}_{\mu_j})^2}; \quad \text{(Standard variation of dispersion mean of module; 10)}$$

Figure 3 shows that this standard deviation reflects the spatial variation of areas inside a given number of stars with $\varepsilon = 1$ (ψ_a), in contrast with a second set of stars with $\varepsilon = 0.8$ (ψ_b). Thus, the eutacticity parameter ε turns out to be useful to determine the spatial variation of areas inside localities (Eq. 10) when two values of eutacticity are compared. The use of modules associate the value ε with spatial organization since the variation of area sub-localties from two different values

of eutacticity represents variation in module area for any sub-locality (Figure 4). Low values of eutacticty imply spatial heterogeneity while high values imply spatial homogeneity.

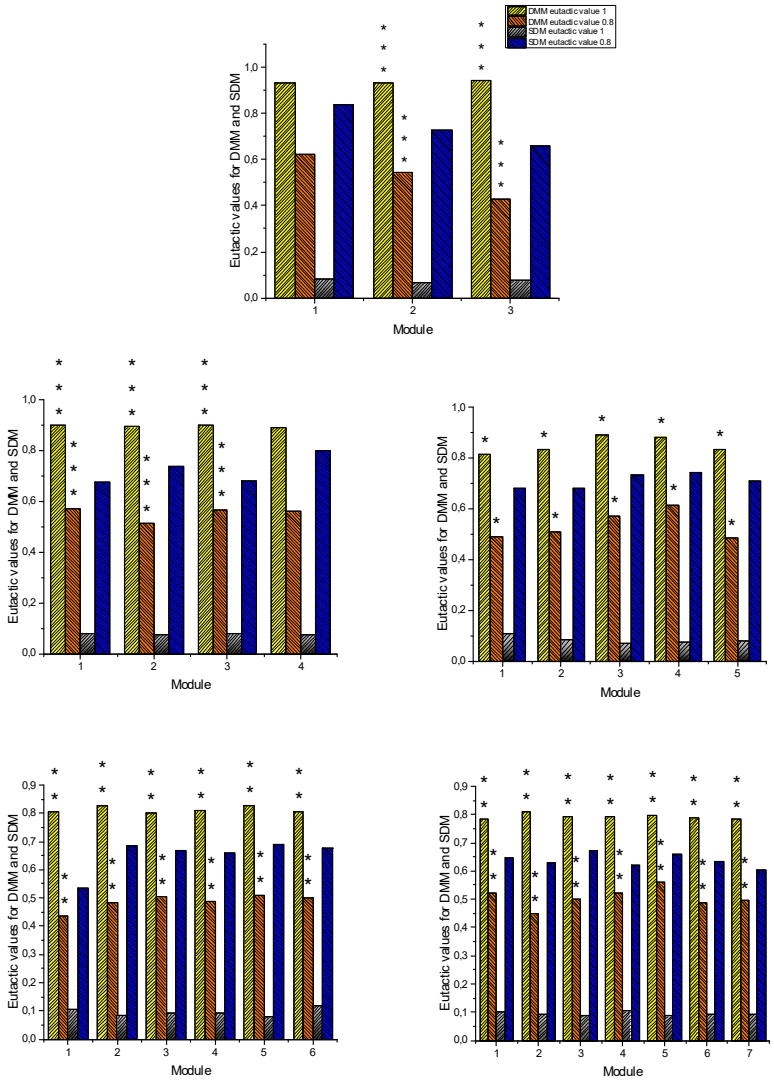

Figure 3. Dispersion mean of modules (DMM) and the standard variation of dispersion mean (SDM). DMM is the average of standard deviation of areas derived from equation 9, from 100 localities using 100 sets of random points with several number of sub-localities with $\varepsilon = 1$ (ψ_a; yellow bars) and $\varepsilon = 0.8$ (ψ_b; orange bars). ANOVA test was performed in order to contrast eutactic values of DMM between ψ_a and ψ_b. The obtained statistical significances of p range from less than 0.0001 for partitions with three modules and four modules (***); less than 0.05 for partitions with 5 modules (*); and less than 0.01 for partitions with 6 and 7 modules (**). The null hypothesis was rejected in 23 of the 25 modules. The SDM (equation 10) for module with $\varepsilon = 1$ (ψ_a; grey bars) is notably smaller than the one obtained from module with $\varepsilon = 0.8$ (ψ_b; blue bars). Figure modified from reference 24.

Preprints (www.preprints.org) | NOT PEER-REVIEWED | Posted: 2 August 2018 doi:10.20944/preprints201808.0042.v1

Peer-reviewed version available at Entropy 2018, 20, 705; doi:10.3390/e20090705

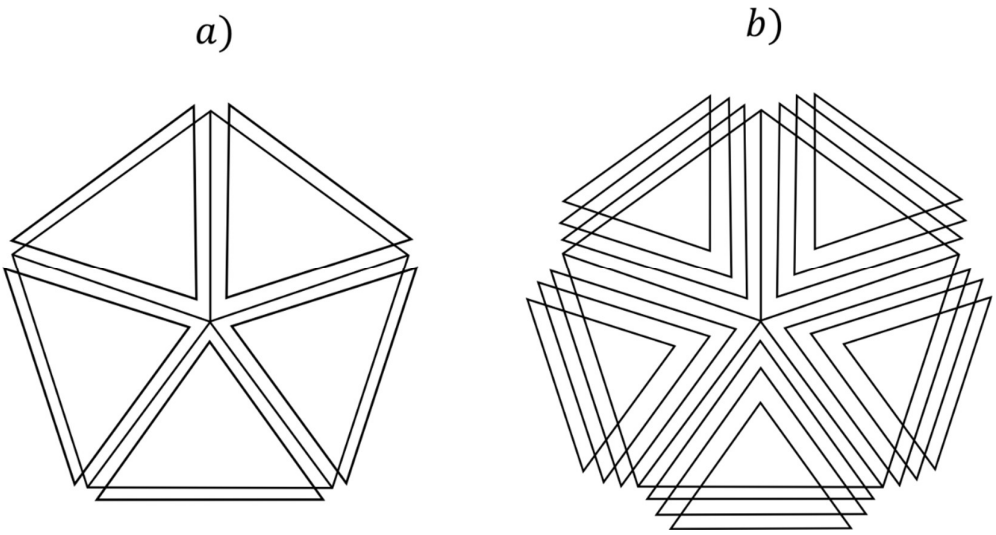

Figure 4. Scheme for area variability of modules defined by regular stars (a) versus modules defined by irregular stars (b) ones. In case (a), low variability in areas (spatial homogeneity derived from standard variation of dispersion mean of module; equation 10) is depicted; this low variability implies non-significant overlap between modules. On the contrary, in case (b) high variability in areas (spatial variability derived from standard variation of dispersion mean of module) is depicted; it implies significant overlap between modules or high variation (modified from reference 24).

Section 2.4 Standard deviation of partition variability

The main objective of our research is to understand the high frequency of five-fold organization in some animal and plants architectures. In past sections 2.1, 2.2 and 2.3 we focused on a computational and quantitative method able to establish some important practical details concerning the measurement of planar spatial variations of shapes Γ. However, to unveil the geometrical properties that favors FO against any other symmetry, we can go beyond by proposing a numerical approach using partitions of planar discs (localities) divided into three to ten sub-localities. In fact, this numerical experiment is necessary to relate equations (1) and (2) with a proper collection of data reflecting a quantification of standard deviations of spatial organization in FO. A complete view of a wide spectrum of partitions of shapes Γ is obtained if we design a numerical model not restricted to the eutacticity parameter, since this parameter is proposed mainly as a tool but it is not a definite proof. Our geometrical design has as a first condition, the fact that planar discs with different number of sub-localities remains with a constant area during the experiment in order to have normalized data. Although we consider partitions of discs ranging from three to ten sob-localities and each partition must be with a constant area during the experiment, we include ten levels of variability. Therefore, each partition with particular constant area has ten levels of variability during the experiment. According to section 2.1, the standard deviation of each locality can be obtained by using equation 2. For this purpose, we use Voronoi diagrams to model space partitioning with different number of parts (from three to ten), where two variables are studied, namely, partitioning number (pn) and partition variability (pv), which are defined as follows:

a) Partitioning number (pn) defines the number of partitions inside a disc (ranging from three to ten).
b) Partition variability (pv) determines multiple levels of variability (ten) inside discs by using random points, which in turn define the Voronoi diagrams. These levels of variability will be defined below.

The algorithm to build partitioning and levels of variability of discs is described in the next **7** steps as follows:

1. We consider initially a disk with a unitary radius where a second inscribed disk will be partitioned into a pn with a pv during the experiment (steps 4 and 5 of this algorithm, respectively). These discs are defined by particular features each: a) The first disc is the external limit of the second and their coordinates are constant during the experiment (b) The second one is constantly changing to obtain a pv (step 5 of this algorithm) and it is obtained by establishing a Voronoi tessellation. These two features a) and b) are described in the next steps 2) and 3) of this algorithm.
2. Features of external disc. The boundaries of the external limit are defined by 24 fixed points generated as follows: The radius of the external disk is set to *r=1* and consecutive points are separated by an angle $\theta/24$. The functionality of this feature lies in the establishment of a fixed limit of reference to maintain a constant area during variation of partitions.
3. Features of internal disc. The boundaries of the internal limit are defined by 24 fixed points generated as follows: The radius of the internal disk is initially set to *r=0.53*±0.4 (established by the first level of variability step 6 of this algorithm) with 24 points consecutively separated by an angle $\theta/24$. These radii are derived from a Voronoi tessellation whose points are the 24 points established before in this step beside the points derived from step 5. The functionality of this feature lies in the establishment of an internal limit able to change, providing statistical variation determining levels of variability of areas inside discs.
4. Now, we define partition numbering (pn) inside the disk. Once a number of partitions is defined, say n (where $3 \leq n \leq 10$ and $n \in \mathbb{Z}$) to define a Voronoi tessellation, points are located in the disk at angles $2\pi/n \pm 0.069$ radians but at different radius. These radius values will define the pv, as described in the next item.
5. Partition variability (pv). For each angular region defined above, 10 points are located at radius (between r=0 and r=10) at different positions to define different degrees of variability using Voronoi tessellations. The first point (first level of variability) is at r=1. After the second point all of them are located at random radius between 1 to 10. Hence, each level of variability (ten) is given by radii ranges except 1 which is fixed at 1 (Figure 5); a) 1, b) 1-2, c) 1-3, d) 1-4, e) 1-5, f) 1-6, g) 1-7, h) 1-8, i) 1-9 and j) 1-10. Partition variability will define the broad spectrum of possibilities for area distribution inside discs without losing partitioning number. According to equation (1) the average of areas requires a summation of sub-localities areas (A_{ij}) which were derived from partitions.
6. Once that partition areas (A_{ij}) inside discs were obtained and equation (1) was solved, equation (2) is used to get standard deviations (σ_i) of variability for each disc. In order to normalize the level of variability for each pn, an index dividing the standard deviation of partitions and the particular area average of each partition was obtained (variability average; supporting information 1). There are eight particular area averages of partitions since we have a sample of 8 discs with different pn (from 3 to 10). These particular area averages are derived from a value n/(≈108.5±1.5) which are n values obtained from the first level of variability (pv) at r=1. It is important to say that the radius of the external disc (1) and the radius of the internal disc (*r=0.53*±0.4) was modified in order to get the particular area averages. However, in spite of the modification the index between external discs and the internal ones remains constant. A sample of 20 discs to get 20 standard deviations $(20\ \sigma_i)$ was generated for each pn, and also for each level of pv (10) giving a sample of 200 discs for each pn. An average of standard deviations $(\bar{\sigma}_i$; variability average) was derived for each level of variability.
7. Finally, a standard deviation of all variability averages is obtained for each pn.

Preprints (www.preprints.org) | NOT PEER-REVIEWED | Posted: 2 August 2018 doi:10.20944/preprints201808.0042.v1

Peer-reviewed version available at Entropy 2018, 20, 705; doi:10.3390/e20090705

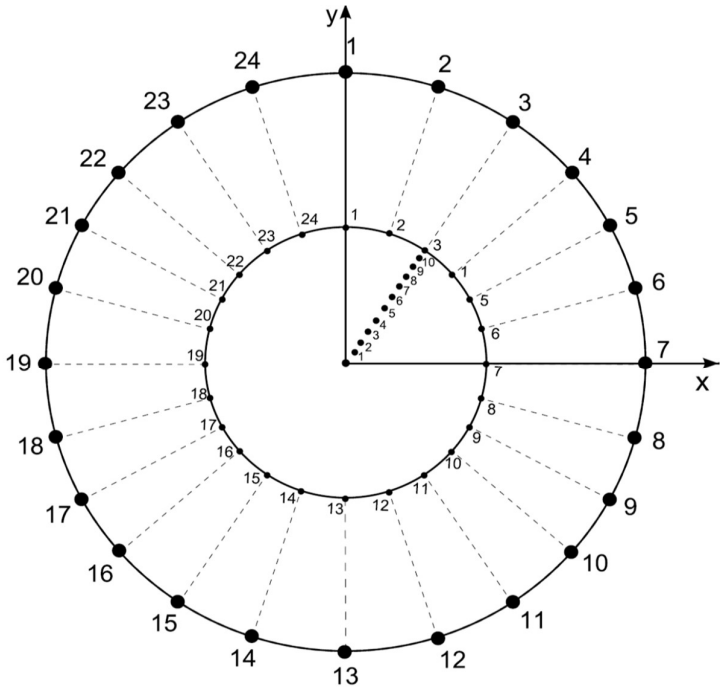

Figure 5. Defining partitioning number and partition variability. A disc is build to get Voronoi diagrams with constant area in spite of variability. The disc of this figure has a partitioning number of 2. The magnitude of the radius defines ten levels of variability; a) 1, b) 1-2, c) 1-3, d) 1-4, e) 1-5, f) 1-6, g) 1-7, h) 1-8, i) 1-9 and j) 1-10. Each level of variability is given by radii ranges except a) which is fixed at 1.

3. Results

Section 3.1 Star morphospace for shapes Γ.

From section 2.3 of methods we can conclude that the higher the eutacticity value the higher the spatial homogeneity inside shapes, that is, less the standard variation of dispersion mean (equation 10; Figure 3). In other words, spatial heterogeneity increases according to the decreasing of eutacticity. In order to define particular values of this property, regarding spatial organization for statistical geometrical samples of several shapes Γ we must build that universe of shapes or star morphospace. Random stars (*n=10,000*), with number of vectors *N= 3, 4, 5, 6, 7, 8, 9* and *10* were generated according to a well established previous methodology reported in reference [24]. Once these sets of stars are generated eutacticity is measured in stars given eight particular statistical distributions (Figure 6). Those distributions are characterized by a mean which will give us a first insight about particular values of spatial organization for shapes Γ which will determine the resulting morphospace (Figure 7). As already has been mentioned in section 2.2, in planar stars the range for eutacticity values is $\frac{1}{\sqrt{2}} \leq \varepsilon \leq 1$, which is a range between 0.7 and 1. A first interesting fact to highlight in figure 6 is that the eutacticity mean value for stars with five vectors (0.89388) is higher than those values for both four and six vectors (0.88126 and 0.88324 respectively). As it was expected from a first eye approach, over the statistical distribution for stars with three vectors (Figure 6.a) the eutacticity value was lower (0.84827) than for all remaining stars (Figure 7 and 8). For stars above seven vectors eutacticity values fall over 0.918. It is important to say at this point that stars with eight, nine and ten vectors can be considered as multiples of degree 2, 3, 4 and 5. However, it is not the case for stars with seven vectors. In fact, structures of seven folding order or higher are rare or absent, except those that can be considered as multiples of the 2, 3, 4 and 5 [11]. Shapes with more

Preprints (www.preprints.org) | NOT PEER-REVIEWED | Posted: 2 August 2018 doi:10.20944/preprints201808.0042.v1

Peer-reviewed version available at Entropy 2018, 20, 705; doi:10.3390/e20090705

than seven vectors can serve as controls to understand spatial deviations from the most abundant stars (3, 4, 5 and 6) although they will be included in our final analysis.

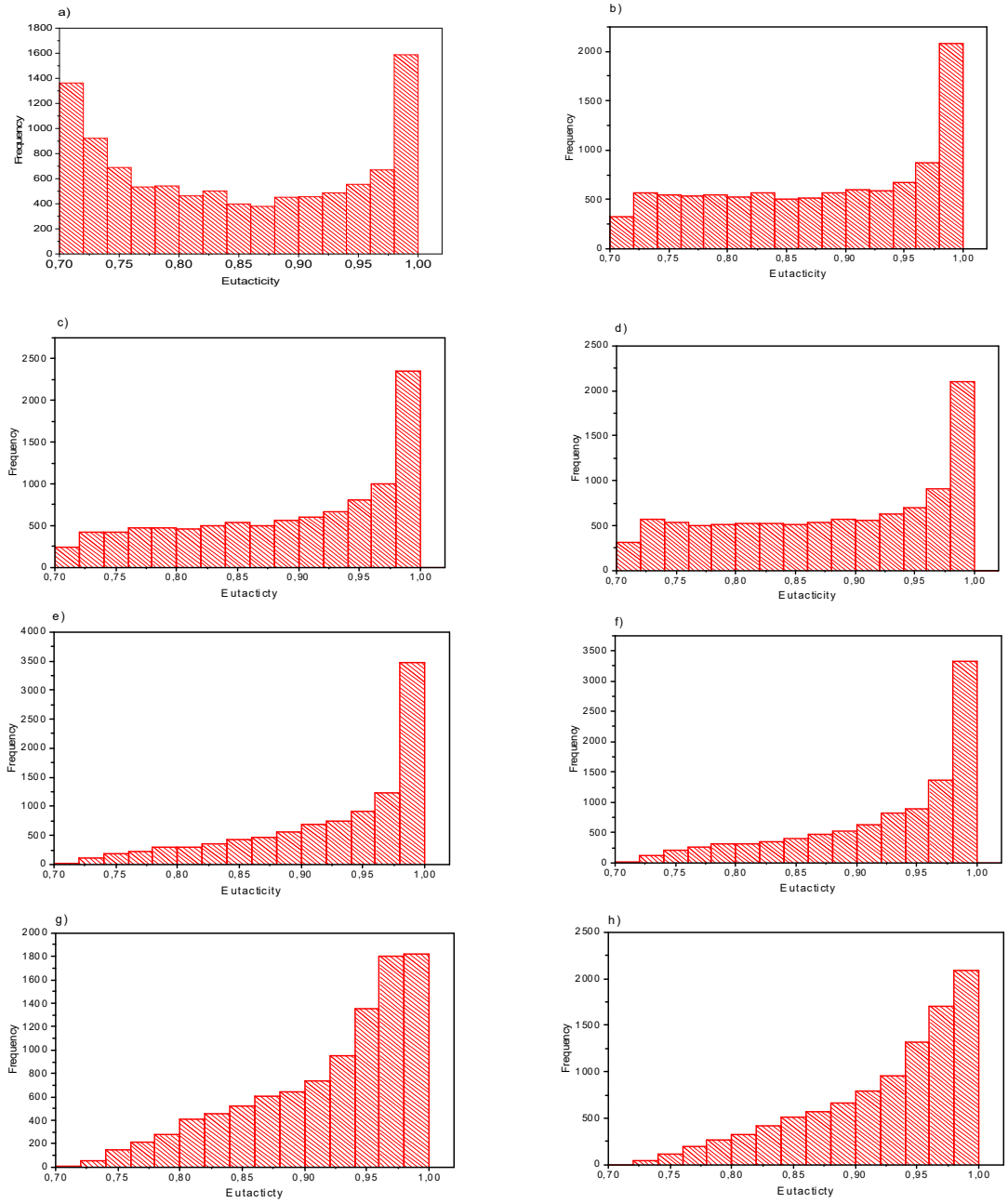

Figure 6. Statistical distributions for random stars showing frequency of eutacticity values. The abscissa indicates eutacticity values (ranging from 0.7 to 1), and ordinate is frequency for vector stars ranging from 3 to 10 vectors (letters from a=3, b=4, c=5, d=6, e=7, f=8, g=9 and h=10).

Preprints (www.preprints.org) | NOT PEER-REVIEWED | Posted: 2 August 2018 doi:10.20944/preprints201808.0042.v1

Peer-reviewed version available at Entropy 2018, 20, 705; doi:10.3390/e20090705

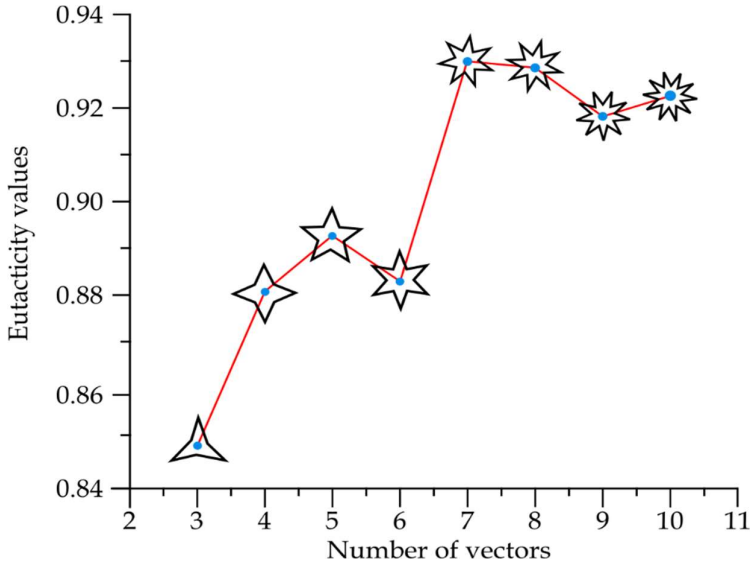

Figure 7. Star morphospace for eutacticity values derived from shapes Γ. Eutacticity means obtained from statistical distributions for vector stars ranging from 3 to 10 vectors.

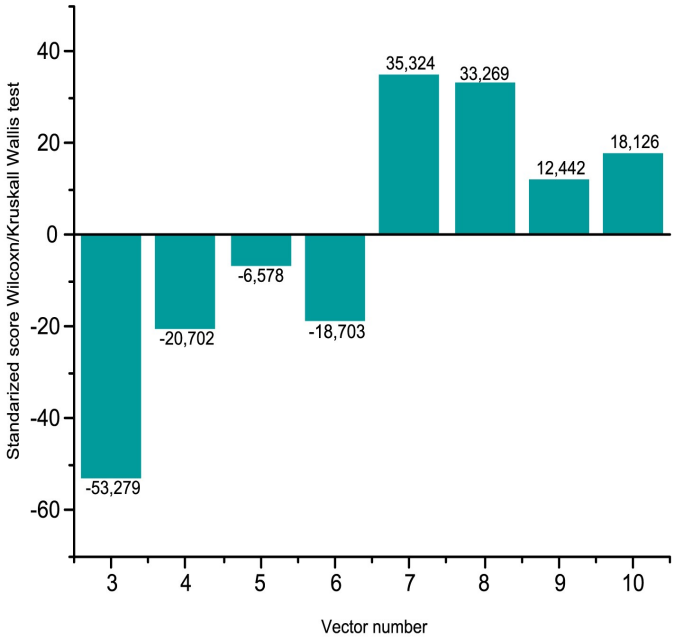

Figure 8. Standardized score Wilcoxon/Kruskall Wallis for vector stars ranging from 3 to 10 vectors. Score for five vector stars is the closest value to zero.

The resulting morphospace comes from the eutacticity values derived from distributions of Figure 6. However, our first result there will not be evident up to the establishment of a formal test comparing distributions. Since we detected that the statistical distributions are non normal (Figure 6), we decided contrast samples using a nonparametric statistical test, the Wilcoxon/Kruskall-Wallis test using the program JMP 8.0. Figure 8 shows the standardized score Wilcoxon/Kruskall Wallis contrasting statistical differences among eutacticity values from all distributions. The Wilcoxon/Kruskall Wallis standardized scores for 3, 4, 5 and 6 vector star distributions fall below the mean while values for seven vectors or more are over the mean. Interestingly, score for five vector stars is the nearest value to zero. This fact reflects the increasing of eutacticity mean for five vector

stars visualized in the morphospace of Figure 7 in the middle of four and six vectors. In addition, four and six vector stars remain closest between them in contrast with five vector stars. Concerning this last point, we focused on comparing only four, five and six vector stars including a statistical analysis contrasting only these samples. Figure 9 shows how distribution of eutacticity values for five vector stars are considerably away from four and six vector star samples. According to this, we can conclude that eutacticity is a suitable measure able to detect variations of spatial organization inside polygons. The average for areas inside regular stars associated to highly eutactic stars reflects a tendency toward equal partition of internal space, while the high variation of SDM indicates that low eutactic stars has a much less equal distribution of areas. In that sense, statistically, five-folding stars are showing that they are in a particular position which is more regular than that for four-folding and six-folding organizations but less than organizations whose vectors are above seven vectors.

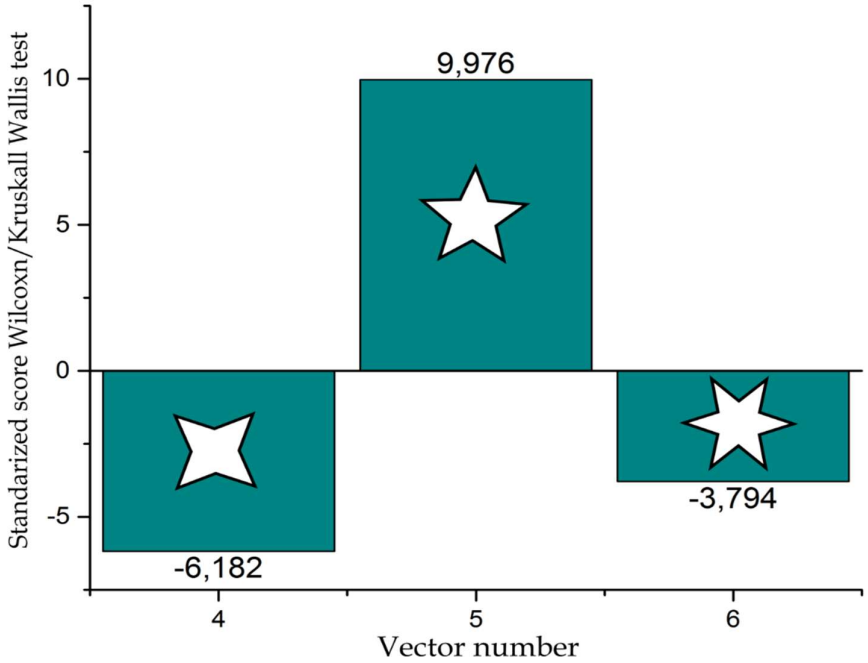

Figure 9. Standardized score Wilcoxon/Kruskall Wallis for vector stars ranging from 4 to 6 vectors. According to the standardized score Wilcoxon/Kruskall Wallis test five vector stars are statistically dissimilar to four and six vectors distributions.

The final part of our methodology (section 2.4) is based on a numerical approach determining particular values for partitions ranging from three to ten sub-localities, using equations (1) and (2). The results of this experiment are shown in Figure 10 and Figure 11. Interestingly, the curves for variability averages between partitions are different (right side squares in Figure 10). Each level of variability was composed of a sample of 20 standard deviations and according to Figure 10 it depends on the partitioning number and level of variation. In addition, the lowest value for standard deviation of the overall sample determined by the variability average is that for five partitioning number. Therefore, we can conclude that equation (2) is an appropriate way to explain that the high frequency of FO in nature is derived from an equal spatial partitioning in spite of spatial variation.

Preprints (www.preprints.org) | NOT PEER-REVIEWED | Posted: 2 August 2018 doi:10.20944/preprints201808.0042.v1

Peer-reviewed version available at Entropy 2018, 20, 705; doi:10.3390/e20090705

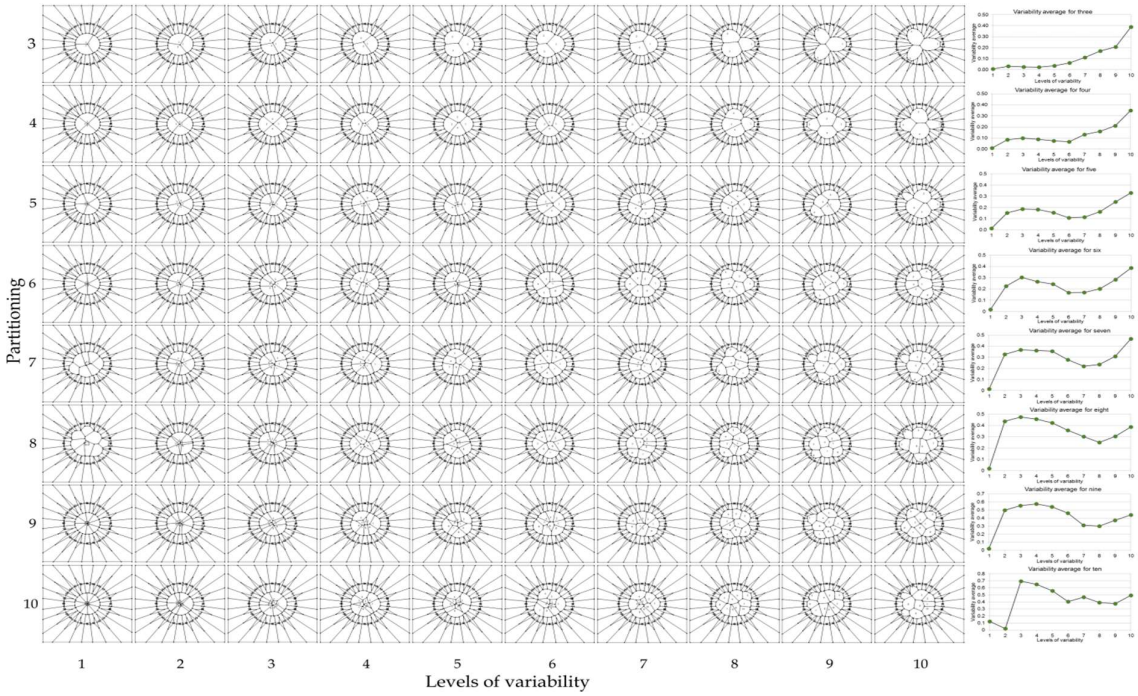

Figure 10. Partitioning number and partition variation of planar discs. A sample of 80 planar discs shows how partitioning number (vertical left side) determines segmentation of an almost constant area (≈108.5±1.5) into particular number of sub-localities. Partition variability (bottom horizontal numbers) installs levels of variability giving ten constant and subtle increases of area to generate random segmentations. Variability averages (right vertical graphics) reflects average of standard deviations ($\bar{\sigma}_i$) which is derived for each level of variability. It is important to note how each increase of variability enhance heterogeneity for every partitioning equally even the graphics are dissimilar.

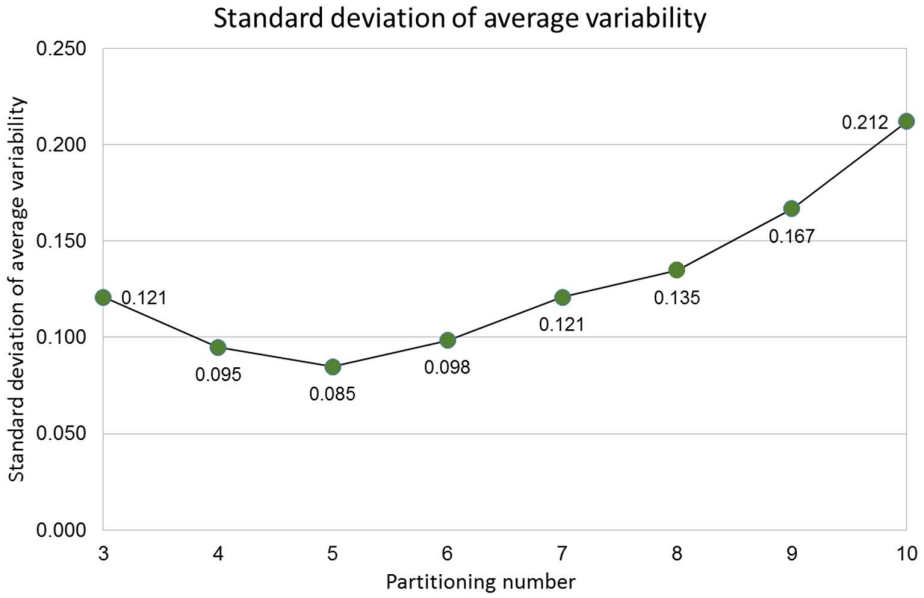

Figure 11. Standard deviation of all variability averages for each partitioning number. An average of standard deviations ($\bar{\sigma}_i$; variability average) was derived for each level of variability from figure 10. A standard deviation of all variability averages is obtained for each partitioning number.

According to this data, five-fold organizations are at the lowest level of dissimilarity among areas inside discs.

4. Discussion

Our final resulting conclusions are that the spatial organization for five-folding architectures or FO can be associated to a particular distribution of homogeneous internal space given by its geometry (Figure 11). That is, our idea lies on a suggestion that geometry defines a source of information and not just is a consequence of traditional physical button-up development. This last idea is notably different from those given by functional, ecological and even mechanical explanations because those hypotheses consider that form follows function. We consider that the significance of our findings is based on the statistical constancy of geometrical constraints, derived from spatial organization of shapes beyond the material or complexity level of many different systems. Our geometrical argument is not against the selective performance for five-folding symmetries in nature, since the high well qualified performance of this geometry during evolution could be a generic geometric constraint defined first as a system character before to be a biological character.

Supplementary Information 1 (Table PDF): In order to normalize the level of variability for each pn, an index dividing the standard deviation of partitions and the particular area average of each partition was obtained (variability average)**.** There are eight particular area averages of partitions since we have a sample of 8 discs with different pn (from 3 to 10). These particular area averages are derived from a value n/(≈108.5±1.5) which are n values obtained from the first level of variability (pv) at r=1. It is important to say that the radius of the external disc (1) and the radius of the internal disc (*r=0.53*±0.4) was modified in order to get the particular area averages. However, in spite of the modification the index between external discs and the internal ones remains constant. A sample of 20 discs to get 20 standard deviations ($20\ \sigma_i$) was generated for each pn, and also for each level of pv (10) giving a sample of 200 discs for each pn. An average of standard deviations ($\overline{\sigma_i}$; variability average) was derived for each level of variability.

Author Contributions: Conceptualization, Juan López Sauceda, Ana Paola Rojas Meza and José Luis Aragón Vera; Methodology, Juan López-Sauceda, Jorge López Ortega, Jacobo Sandoval Gutiérrez and José Luis Aragón Vera; Software, Juan López-Sauceda; Validation, Juan López Sauceda, Jorge López Ortega, Jacobo Sandoval Gutiérrez and José Luis Aragón Vera; Formal Analysis, Juan López-Sauceda, Jorge López Ortega, Jacobo Sandoval Gutiérrez, Gerardo Abel Laguna Sánchez, Ana Paola Rojas Meza and José Luis Aragón Vera; Investigation, Juan López-Sauceda, Jorge López Ortega and Gerardo Abel Laguna Sánchez; Resources, Juan López-Sauceda; Data Curation, Juan López-Sauceda, Jorge López Ortega; Writing-Original Draft Preparation, Juan López-Sauceda and Ana paola Rojas Meza; Writing-Review & Editing, Juan López-Sauceda, Jorge López Ortega, Jacobo Sandoval Gutiérrez, Gerardo Abel Laguna Sánchez, Ana Paola Rojas Meza and José Luis Aragón Vera; Visualization, Juan López-Sauceda, Jorge López Ortega, Jacobo Sandoval Gutiérrez and Jose Luis Aragón Vera; Supervision, Juan López-Sauceda; Project Administration, Juan López-Sauceda, Jacobo Sandoval Gutiérrez, Gerardo Abel Laguna Sánchez and Ana Paola Rojas Meza; Funding Acquisition, Juan López-Sauceda, Jorge López Ortega, Jacobo Sandoval Gutiérrez, Gerardo Abel Laguna Sánchez.

Funding: The authors gratefully acknowledge the financial support from Mexican National Council for Science and Technology.

Conflicts of Interest: The authors declare no conflict of interest.

References

1. Darvas, G.; *Symmetry: Cultural-historical and ontological aspects of Science-Arts relations; the natural and man-made world in an interdisciplinary approach,* 1st ed.; Birkhauser: Berlin, Germany, 2007; pp. 171-191, 978-3-7643-7554-6.

2. Arenas-Mena, C.; Cameron, A. R.; Davidson, E. H., Spatial expression of Hox cluster genes in the ontogeny of a sea urchin. *Development* **2000,** *127* (21), 4631-4643.

3. Mooi, R.; David, B., Radial Symmetry, the Anterior/Posterior Axis, and Echinoderm Hox Genes. *Annual Review of Ecology Evolution and Systematics* **2008,** *39*, 43-62. DOI 10.1146/annurev.ecolsys.39.110707.173521.

4. Brown, W. M.; Price, M. E.; Kang, J. S.; Pound, N.; Zhao, Y.; Yu, H., Fluctuating asymmetry and preferences for sex-typical bodily characteristics. *Proceedings of the National Academy of Sciences of the United States of America* **2008,** *105* (35), 12938-12943. DOI 10.1073/pnas.0710420105.

5. Hotchkiss, F. H. C., On the number of rays in starfish. *American Zoologist* **2000,** *40* (3), 340-354. DOI 10.1668/0003-1569(2000)040[0340:otnori]2.0.co;2.

6. Martindale, M. Q.; Finnerty, J. R.; Henry, J. Q., The Radiata and the evolutionary origins of the bilaterian body plan. *Molecular Phylogenetics and Evolution* **2002,** *24* (3), 358-365. DOI 10.1016/s1055-7903(02)00208-7.

7. Moller, A. P.; Eriksson, M., POLLINATOR PREFERENCE FOR SYMMETRICAL FLOWERS AND SEXUAL SELECTION IN PLANTS. *Oikos* **1995,** *73* (1), 15-22. DOI 10.2307/3545720.

8. Moller, A. P.; Sorci, G., Insect preference for symmetrical artificial flowers. *Oecologia* **1998,** *114* (1), 37-42. DOI 10.1007/s004420050417.

9. Popodi, E.; Raff, R. A., Hox genes in a pentameral animal. *Bioessays* **2001,** *23* (3), 211-214. DOI 10.1002/1521-1878(200103)23:3<211::aid-bies1030>3.0.co;2-6.

10. Smith, A. B., Deuterostomes in a twist: the origins of a radical new body plan. *Evolution & Development* **2008,** *10* (4), 493-503. DOI 10.1111/j.1525-142X.2008.00260.x.

11. Breder, C. M.; Observations on the occurrence and attributes of pentagonal symmetry. *Bulletin of The American Musuem of Natural History* **1955,** 106: 173-220.

12. Hargittai, I.; *Fivefold Symmetry,* 1st ed.; World Scientific: Farrer Road, Singapure, 1994; pp. 11-23, 978-9810206000.

13. Smith, J. M.; Burian, R.; Kauffman, S.; Alberch, P.; Campbell, J.; Goodwin, B.; Lande, R.; Raup, D.; Wolpert, L., DEVELOPMENTAL CONSTRAINTS AND EVOLUTION. *Quarterly Review of Biology* **1985,** *60* (3), 265-287. DOI 10.1086/414425.

14. Raff, R. A.; *The Shape of Life: Genes, development, and the evolution of animal form,* 1st ed.; The University of Chicago Press: Chicago, USA, 1996; pp. 38-61, 978-0226702667.

15. Stephenson, D. G., PENTAMERAL SYMMETRY IN ECHINODERMS. *Nature* **1967,** *216* (5119), 994-+. DOI 10.1038/216994a0.

16. Grabowsky, G. L., SYMMETRY, LOCOMOTION, AND THE EVOLUTION OF AN ANTERIOR END - A LESSON FROM SEA-URCHINS. *Evolution* **1994,** *48* (4), 1130-1146. DOI 10.2307/2410373.

17. Aragon, J. L.; Torres, M.; Gil, D.; Barrio, R. A.; Maini, P. K., Turing patterns with pentagonal symmetry. *Physical Review E* **2002,** *65* (5). DOI 10.1103/PhysRevE.65.051913.

18. Lopez-Sauceda, J.; Aragon, J. L., Eutacticity in sea urchin evolution. *Bulletin of Mathematical Biology* **2008,** *70* (2), 625-634. DOI 10.1007/s11538-007-9273-2.

19. Chen, E. R.; Klotsa, D.; Engel, M.; Damasceno, P. F.; Glotzer, S. C., Complexity in Surfaces of Densest Packings for Families of Polyhedra. *Physical Review X* **2014,** *4* (1). DOI 10.1103/PhysRevX.4.011024.

20. Damasceno, P. F.; Engel, M.; Glotzer, S. C., Predictive Self-Assembly of Polyhedra into Complex Structures. *Science* **2012,** *337* (6093), 453-457. DOI 10.1126/science.1220869.

21. Wagner, G. P., Homologues, natural kinds and the evolution of modularity. *American Zoologist* **1996,** *36* (1), 36-43.

22. Fontana, W.; Buss, L. W., THE ARRIVAL OF THE FITTEST - TOWARD A THEORY OF BIOLOGICAL ORGANIZATION. *Bulletin of Mathematical Biology* **1994,** *56* (1), 1-64.

23. McGhee, G.; *The Geometry of Evolution: Adaptative Landscapes and Theoretical Morphospaces,* 1st ed.; Cambridge University Press: United Kingdom, 2006; pp. 57-65, 978-0521849425.

24. Lopez-Sauceda, J.; Malda-Barrera, J.; Laguarda-Figueras, A.; Solis-Marin, F.; Aragon, J. L., Influence of Modularity and Regularity on Disparity of Atelostomata Sea Urchins. *Evolutionary Bioinformatics* **2014,** *10,* 97-105. DOI 10.4137/ebo.s14457.

25. Lopez-Sauceda, J.; Rueda-Contreras, M. D., A Method to Categorize 2-Dimensional Patterns Using Statistics of Spatial Organization. *Evolutionary Bioinformatics* **2017,** *13*. DOI 10.1177/1176934317697978.

26. Coxeter, H. S. M.; *Regular Polytopes,* 2nd ed.; Dover: New York, USA, 1973; pp. 15-20, 0-486-61480-8.

27. Torres, M.; Aragon, J. L.; Dominguez, P.; Gil, D., Regularity in irregular echinoids. *Journal of Mathematical Biology* **2002,** *44* (4), 330-340. DOI 10.1007/s002850100126.